Spreading and contact-line arrest dynamics of impacting oxidized liquid-metal droplets

Ryan McGuan [1,*] Robert N. Candler [2,3] and H. Pirouz Kavehpour[1]

[1]*Department of Mechanical and Aerospace Engineering,*
University of California, Los Angeles, California 90095, USA
[2]*Department of Electrical and Computer Engineering,*
University of California, Los Angeles, California 90095, USA
[3]*California NanoSystems Institute, Los Angeles, California 90095, USA*

Gallium based room temperature liquid metal alloys present an exciting opportunity for research due to their attractive material properties. These alloys can readily remain liquid at room temperature and exhibit unusual phenomena at the air-liquid interface due to oxidation of the gallium. We present a phenomenological study of droplet impacts on a solid substrate measuring the spread parameter $\xi_{\max} = D_{\max}/D_0$ as function of the Weber number, and by extension, the impact velocity, as well as the spread time of the droplets. In order to characterize the surface behavior, we utilized direct measurement of surface forces using a glass probe and a tensiometer, finding the effective surface tension to be $\sigma_{\mathrm{eff}} = 628 \pm 37$ mN/m. Finally, we developed a model of spreading that scales the spread factor $\xi_{\max}$ with the Weber number to the power of $\frac{1}{2}$.

I. INTRODUCTION

Gallium alloys have received attention due to their vast array of applications, particularly in the fields of electronics, microfluidics, biomedical engineering, and chemistry [1–3]. They are often called room temperature liquid metals (RTLMs), a term coined by Dickey, whose group has done a great deal of research about these alloys [4–6]. These metals tend to be gallium based and are often combined with indium, usually called EGaIn, as well as tin, commercially known as Galinstan [7,8]. This research focused on a eutectic alloy comprising 68.5% gallium, 21.5% indium, and 10% tin, known commercially as Galinstan, and is available commercially from Geratherm Medical. While there have been studies of certain properties of RTLMs such as viscosity μ, and the effect of oxidation on the surface tension σ, there is still a need to understand the effects of surface oxidation for dynamic events and to develop a predictive model for these effects [9]. Xu *et al.* performed droplet impacts with a similar liquid metal, EGaIn, focused on the effect of acid wash vs the oxidized case [10], but that study utilized bulk rheology to quantify elastic effects in order to modify the impacting Weber number to collapse the data. In this work we take a different approach in studying a different alloy and in how we model the skin effect, instead treating it like a Hookean mechanical spring. The focus of this manuscript is on the impacts of droplets and how features such as the droplet volume V and the impact velocity V_0 affect the spread factor $\xi_{\max} = D_{\max}/D_0$, and spread time t_s, and to present a model for this behavior. This will also be cast in terms of the Weber number $\mathrm{We} = \rho V^2 D_0/\sigma$ and Reynolds number $\mathrm{Re} = \rho V D_0/\mu$ where ρ is the liquid metal density and other variables are as mentioned previously.
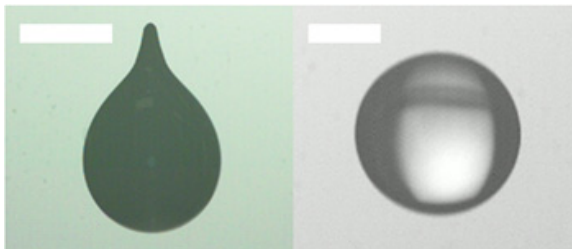
*rmcguan@gmail.com

FIG. 1. (Left) RTLM droplet in flight with 2 mm scale bar. Shape is maintained through entire falling sequence. (Right) Water droplet in flight with 1 mm scale bar.

II. OXIDATION EFFECTS

Critical to understanding the behavior of RTLMs is the study of oxidation occurring at the surface. There is some disagreement about the surface tension of this commonly used formulation with the value presented as between 517 and 718 mN/m [11,12]. Many authors attribute this difference to different formulations (e.g., from additives) but it also may be due to the use of different techniques for measuring apparent surface tension and complications caused by the oxide layer. The gallium oxides that form at the surface form a "skin" that is self-limiting, insulating the bulk material from further oxidation, and generally remains between 0.5 and 3 nm thick [13]. Despite being very thin, this oxide layer stores energy and resists typical capillary phenomena such as the minimization of surface area as shown in Fig. 1. This skin layer has dramatic effects regarding both the way the fluid flows and interfacial phenomena such as surface minimization, Plateau-Rayleigh instabilities, and coronal instabilities [14,15].

It is often reported that gallium alloys wet glass and other similar surfaces when actually RTLMs do adhere to glass due to the skin, but they do not spread due to capillary forces, only due to gravity and mechanical work. In fact, when oxidation is prevented, such as in an inert environment, the advancing contact angle θ_a is 146.8° and the receding contact angle θ_r is 121.6° indicating a highly nonwetting liquid [12].

Correctly quantifying surface vs bulk forces is important when understanding the mechanics of RTLMs. The value of $\sigma = 718$ mN/m is commonly reported as the surface tension of oxidized Galinstan due to the oxidation layer. The apparent surface tension is a strong function of the measurement method used as well as the method by which the droplet surfaces are created [16]. For example, in another study Kocourek found the surface tension of this composition to be $\sigma = 517$ mN/m using a contact angle method [17]. This leads to a range of values spanning 200 mN/m in the literature.

If we think of the skin and bulk fluid as separate materials—the literature seems to indicate that they are quite distinct—then some interfacial tension exists between the bulk fluid and the gallium oxide layer. This skin also has its own material properties, namely, elasticity, which means that not only does it add additional tensile stress when the surface is expanded, but it also resists changes that decrease the local surface area. Nominally surface tension will always cause a fluid to tend to the minimum surface area in the absence of other forces of significant magnitude, but with liquid metal this is not always the case. Modeling the skin properly may actually be more complicated than is often acknowledged. For example, simple procedural changes may produce different results. If the pendant drop method was carried out and the drop was created and then reduced slightly in size before measurements were taken, this may produce different results than if the droplet was created to the second size alone due to energy storage in the skin. To account for this complication, we chose to measure the mechanical force at the contact line using a direct method, tensiometry, rather than sessile droplet or pendant droplet methods.

We utilized a Krüss Scientific K100 tensiometer and employed a common method of tensiometry known as the Whilemy plate method, modified to incorporate a glass rod. Due to gallium's

TABLE I. Material properties of liquid metal eutectic. Formulation is 68.5% Ga, 21.5% In, and 10% Sn [11,19].

Boiling point	1300 °C	Melting point	−19 °C
Vapor pressure	$<1.33 \times 10^{-6}$ Pa	Density	6.44 g/cm^3
Surface tension	628 ± 37 mN/m	Viscosity (bulk)	0.0024 Pa s

propensity to form amalgams with many metals, this method was modified to utilize a glass rod which mimics the substrate material on which the impacts occurred. It was also found the rod geometry produced more repeatable results than a plate geometry due to the material remaining adhered to the edges of the plate [18]. The RTLM was washed with 1 M NaOH prior to testing and clean metal was placed in the testing container, exposed to air. Testing was carried out after enough time had passed to allow for oxidation at the surface (>5 min) and such that oxidation was confined to the surface. The glass rod was inserted into the liquid metal and withdrawn at a rate of 3 mm/min until a maximum force was achieved which, with the length of the contact line, was used to calculate the surface tension. The value for the effective surface tension σ_{eff} was found to be 628 ± 37 mN/m. This value falls within the range established by the literature, appearing closer to the middle of accepted values. $\sigma_{\text{eff}} = 628$ mN/m is the value we used for calculation in this manuscript and this value as well as other material properties are listed in Table I.

III. SCALING OF DROPLET IMPACTS

The study of impacting droplets provides an opportunity to investigate the relative effects of various fundamental forces in fluid mechanics including viscous, interfacial, gravity, and inertial forces [20]. It is also useful for designing and fine-tuning droplet based methods of manufacturing with metals [21]. The most common model for droplet impact and the spreading ξ was derived by Pasandideh-Fard *et al.* [22]:

$$\frac{D_{\text{max}}}{D_0} = \xi_{\text{max}} = \sqrt{\frac{\text{We} + 12}{3(1 - \cos\theta_a) + 4(\text{We}/\sqrt{\text{Re}})}}, \tag{1}$$

which was derived by equating the impacting kinetic and surface energies with the viscous dissipation as well as the work of spreading. This relationship can be reduced as follows:

$$\xi_{\text{max}} = 0.5\text{Re}^{0.25} \quad \text{or} \quad \xi_{\text{max}} \sim V^{0.25}. \tag{2}$$

Equation (2) applies for cases where $\text{We} \gg \sqrt{\text{Re}}$ and if $\text{We} \gg 12$. Pasandideh-Fard derived this by modeling the work of spreading per Carey, who notes that nonwetting liquids require much more work to spread, given by [23]

$$W_{sp} = \sigma A[1 - \cos(\theta_a)], \tag{3}$$

where A is the wetted area and W_{sp} is the work associated with spreading. This model is applicable for many typical surfaces however it underpredicts the power law scaling term of the spreading if the surface is sufficiently nonwetting. For example, water on a hydrophobic surface will scale differently from the model in Eq. (4) for a given impact velocity, and by extension, Weber and Reynolds numbers. Clanet *et al.* studied water drops impacting on solid surfaces with superhydrophobic coatings [24]. In this analysis they were able to determine that viscosity had a negligible effect, likely due to slip length at the interface, and constructed a model based on the capillary length with the impact deceleration taking the place of gravity, producing a "gravity puddle." The result was
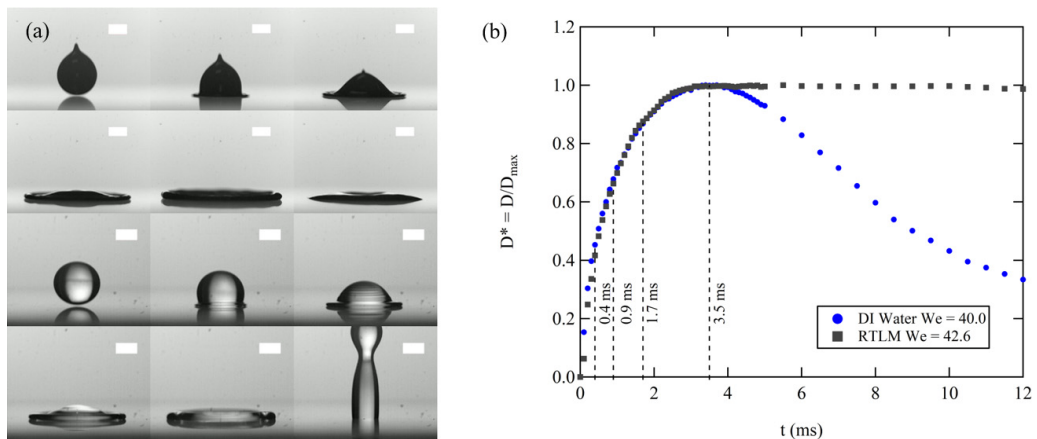
FIG. 2. (a) Impact sequence of liquid metal droplets at We = 42.6 (top) and DI water droplets at We = 40.0 (bottom) on hydrophobic substrate. Time stamps are 0, 0.4, 0.9, 1.7, 3.5, and 15.4 ms for both sequences. Scale bar indicates 1 mm. (b) The same sequence normalized by D_{max}; note that ξ_{max} is not the same for both datasets.

found to scale as

$$\xi_{max} \sim We^{0.25} \quad \text{or} \quad \xi_{max} \sim V^{0.5}, \tag{4}$$

with the coefficient of proportionality being 0.9. Equation (4) indicates as the Weber number, We, increases, there is a decidedly different change in ξ_{max} as compared to Eq. (1). It also should be noted that due to the hydrophobicity ξ_{max} does not represent the final diameter as the droplets would rebound and even bounce at sufficiently high enough impact velocities [25]. Of note is that Clanet's paper did speculate that in an elastic impact $\xi_{max} \sim We^{0.5}$ or $\xi_{max} \sim V$, but was not able to confirm this empirically and then went on to derive the aforementioned model.

Although the results listed in Eq. (4) seem to indicate an effective conversion of kinetic energy to maximum spread, the process is complicated by the rebounding and bouncing nature after maximum deformation. One might expect the fluid to rebound due to high surface tension as in Clanet's work, but the oxide layer adheres to the glass. Furthermore the oxide layer has a degree of elasticity and provides mechanical stability for the deposited material and has been demonstrated to produce freestanding liquid structures [16,26]. There has been very little study of these liquids in the field of droplet impact. Xu *et al.* studied a similar alloy, EGaIn; however, they observed a different relationship than that described by this work. Their study involved two different nozzle sizes for the generation of oxidized liquid metal droplets. The larger nozzle produced droplets that were significantly larger than the range tested here, with a Bond number Bo = $\rho g D_0^2/\sigma$ of 22 while the largest tested here is Bo = 1.2, making it difficult to properly compare these datasets. The smaller nozzle size did produce droplets within the size range we investigated and can be shown to fit the model if the difference in measurement methodologies is accounted for.

Figure 2 shows the impact sequence for a liquid metal droplet on a glass substrate and de-ionized (DI) water on a hydrophobic substrate. The droplets were matched by Weber number and the impact sequences look quite similar until $D = D_{max}$, at which point the water begins to rebound while the metal droplet is pinned in place due to the oxide glass adhesion. This is a sign that bulk viscosity plays a small or negligible role similar to Clanet's observations. Schiaffino and Sonin studied droplet impacts over a range of We and Ohnesorge numbers, Oh, and created four categories of droplet impact by the resisting and driving forces. Based on the material properties of the RTLM and the impact conditions, all of the impact sequences tested could be considered impact driven (as opposed to capillarity) and inviscid as shown by region I in Fig. 4(b) below [27].
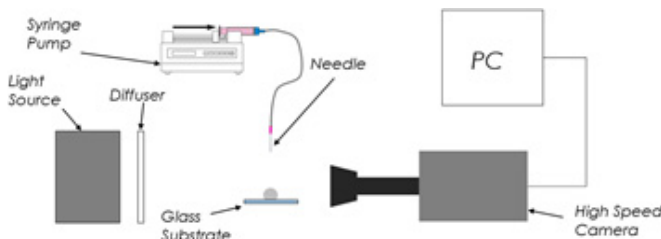
FIG. 3. Experimental setup for droplet impact experiments.

IV. METHODS

Our test setup for the droplet impact testing included a stepper motor controlled Z axis in order to adjust the height and impact velocity. A Phantom V7.2 (Vision Research) high-speed camera was mounted to an optical table and lit with a high-power LED backlight and diffuser. A Kent Scientific Genie Plus syringe pump was used to pump RTLM out of needles composed of the composites polytetrafluoroethylene (PTFE) or polypropylene in order to ensure there was no chemical reaction between the metal and the dispensing needle. Three needle sizes were used in order to modulate the droplet volume, a 20-, 25-, and 30-gauge needle. We also performed comparative experiments of water droplets impacting a hydrophobic substrate. These results were comparted to Clanet's work and found to fit the model. Every impact sequence was shot at 10 000 frames per second and image analysis was carried out with IMAGEJ software with spatial resolution of 17–20 μm. The setup is shown in Fig. 3.

Due to the oxide layer's presence the droplets in flight did not minimize surface area and assume a spherical shape. The droplets had different shapes when dispensed from the different needle sizes but did remain consistent in shape and volume as well as remaining axially symmetric in all cases. Xu *et al.* take a similar approach but select the maximum width of the droplet. We were concerned about shape effects as droplets produced from the different needle gauges were not only different sizes but had different overall shapes. In order to account for shape effects, the droplet volumes were used and a sphere equivalent diameter D_0 was chosen as follows:

$$D_0 = \left(\frac{6}{\pi} \mathcal{V}\right)^{1/3},$$

(5)

where the volume $\mathcal{V}$ was determined by image analysis using IMAGEJ software. For all background information and for DI water impacts in this document D_0 refers to the droplet flight diameter.

For RTLM, D_0 is given by Eq. (5) but D_0 refers to the flight diameter when discussing other droplets such as the water droplet. The three needle sizes were chosen in order to study the effects of droplet volume. The average volume for the 20G was 22.38 μl giving $D_0 = 3.50$ mm, for the 25G was 10.73 μl giving $D_0 = 2.74$ mm, and for the 25G was 6.85 μl giving $D_0 = 2.35$ mm.

The droplet impacts were carried out for a range of conditions $10.7 \leqslant \text{We} \leqslant 205.5$ and $4270 \leqslant \text{Re} \leqslant 19\,979$. For all impacts there were no satellite droplets observed and only minor fingering at the highest Weber numbers. The adhesion of the oxide layer to the substrate meant the final diameter was equal to $D_{\max}$; in other words there was no retraction or rebound.

V. IMPACT MODEL

Due to the fact that oxidation is confined to the surface, the dynamics can be considered quite complicated if fully parsed out. There is adhesion between the skin and the glass substrate, the mechanical properties of the skin itself, and interfacial energy between the oxide skin and the nonoxidized bulk, as well as the bulk viscosity and inertia to contend with. We have found that a simplified model is sufficient to explain this complicated interaction.
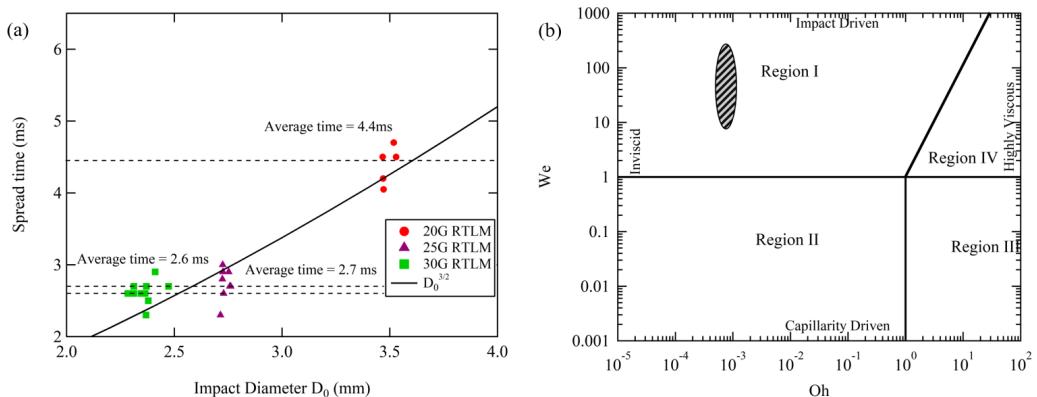
FIG. 4. (a) Droplet spread time vs impact diameter D_0. (b) Droplet impact regions as defined by Schiaffino and Sonin [27].

We begin by assuming that the net result of these forces is a restoring force, F_{rest}, that acts at the contact line that follows scales as the Hookean model with the length of the contact line and the effective surface tension [28]:

$$F_{rest} \sim \sigma_{eff} \, \pi (D - D_{eq}),\qquad(6)$$

where D_{eq} represents the equilibrium position, the state of zero tension or compression. As the diameter D increases the restoring force increases linearly, albeit with an offset D_{eq}. This offset can be observed empirically by depositing the droplets directly onto the substrate so that $V_0 \approx 0$ and therefore We $= 0$. In doing this we found the equilibrium diameter as a function of D_0 to be $D_{eq} = 0.6 D_0$. We then seek to develop the energy associated with this term as the droplet spreads; we do this by integrating the force over the path:

$$SE = \int F_{rest}dx = \sigma_{eff} \, \pi C \int (D - 0.6D_0)\, d(D - 0.6D_0) = \frac{\sigma_{eff}\, \pi C}{2}(D - 0.6D_0)^2,\qquad(7)$$

where C is a constant that will serve as a scaling term (see Fig. 4).This expression can be used in a conservation of energy equation following the method described by the energy balance described in Chandra's work [29] while dropping the viscous term and including the term from Eq. (7).

$$KE_1 = KE_2 + SE.\qquad(8)$$

At maximum spread $KE_2 = 0$ and the SE term is taken at $D = D_{max}$ giving the following expression:

$$\frac{1}{2}\rho \Psi V_0^2 = \frac{\sigma_{eff}\, \pi C}{2}(D_{max} - 0.6D_0)^2.\qquad(9)$$

FBy leveraging the definition of $\xi_{max} = D_{max}/D_0$ and solving for ξ_{max}, Eq. (9) becomes

$$\xi_{max} = A\text{We}^{1/2} + 0.6,\qquad(10)$$

where A is a constant of proportionality that will be fitted from the data. Strikingly, the scaling for this model is quite different from those of both Pasandideh-Fard's group and Clanet's and instead follows the scaling relationship:

$$\xi_{max} \sim \text{We}^{0.5} \quad \text{or} \quad \xi_{max} \sim V.\qquad(11)$$
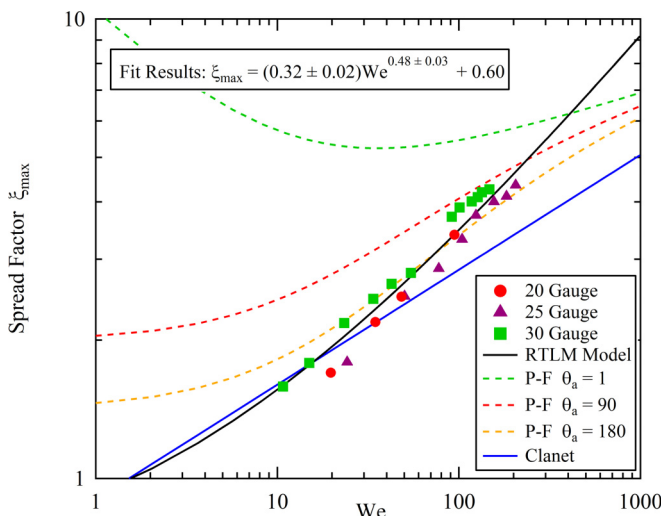
FIG. 5. Comparison of spread factor scaling models and impact data. Green, red, and orange dashed lines are the Pasandideh-Fard model for normal surfaces [22] for advancing contact angles of 1°, 90°, and 180° respectively; the solid blue line is the Clanet model for water on a superhydrophobic surface [24]; and the solid black line is this work. The markers indicate the impact data and are differentiated by needle size.

VI. RESULTS AND DISCUSSION

Figure 5 shows the data from the droplet impact experiments plotted with impact Weber numbers vs the spread factor $\xi_{\max}$. The model was fit with the IGOR PRO software from Wavemetrics and obeys the fit equation $\xi_{\max} = y0 + A(\text{We})^{pow}$ with A found to be 0.32 ± 0.02 and pow found to be 0.48 ± 0.03. This linear relationship with velocity contrasts starkly with the other models as detailed in Fig. 5. This figure shows all three models including a range of advancing contact angles for the Pasandideh-Fard model. Our model performs similarly to the Clanet model at lower Weber numbers but predicts greater spreading than all three as the We $\rightarrow$ 200. This conflicts with reality for a substance that is fully wetting but it should be noted that the Pasandideh-Fard model loses utility as $\theta_a \rightarrow 0^+$ and is included only to show the extrema of the model.

Another facet of this elastic relationship is that the spread time is independent of the impact velocity as seen in Fig. 4(a). The droplet's impacts are clustered per needle size and, by extension, their volume or D_0. The velocity independence of time not only conforms to predictions by the model as listed in Eq. (11), but also matches the results for Clanet's work mentioned previously. The average t_s was found to be 2.6 ms for the 30-gauge needle, 2.7 ms for the 25-gauge needle, and 4.4 ms for the 20-gauge needle.

Impact and initial spreading velocities are assumed to scale with each other so the spread factor would increase linearly with velocity if spread time is constant for a given D_0. This conforms to the linearly elastic assumption applied to derive Eq. (7) since time to maximum is a function of mass and, presumably in this case, σ_{eff} only and independent of V_0. The one caveat with this model is that the contact line is pinned at maximum. This we believe is due to the adhesive nature of the skin and not due to dissipation of energy due to viscosity as the droplet can be seen to oscillate even after reaching a maximum value and becoming pinned. The predicted spread time from linear elastic theory would scale as $t_s \sim \sqrt{m/k}$ or, in this case, $t_s \sim D_0^{3/2}\sigma_{\text{eff}}^{1/2}$ which is depicted in Fig. 4(a).

Figure 6 shows six different impact events chosen to represent two groupings of We and showcasing the range of volumes tested. The figure shows that the spread behavior is similar for droplets of similar volumes regardless of We. For example, the larger droplets take much longer to spread as compared to the lower droplet volumes regardless of impact velocity. The different
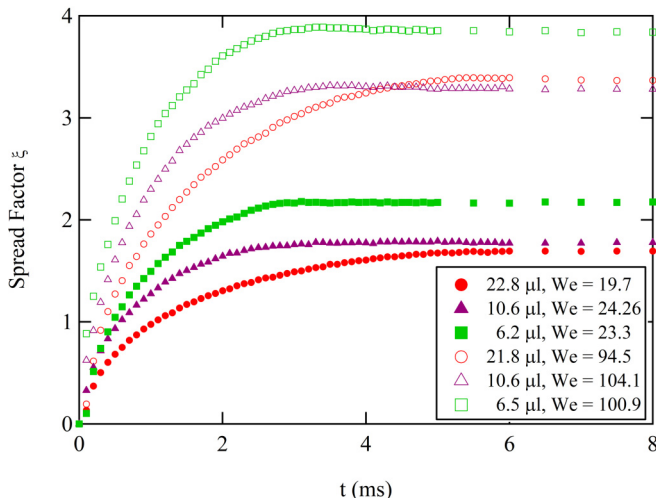
FIG. 6. Spread factor ξ vs time for six different impacts. Red represents the 20G needle with filled circles corresponding to 22.8 μl droplet at We = 22.3 and open circles are 21.8 μl at We = 106.9. Blue represents the 25G needle with filled triangles at 10.6 μl and We = 27.4 and open triangles at 10.6 μl and We = 117.8. Green represents the 30G needles with filled squares at 6.2 μl at We = 27.4 and open squares at 6.5 μl and We = 114.1.

droplet volumes also group well by We number. This similarity of spread behavior for droplets of similar mass independent of impact velocity is characteristic of the linear elasticity we posited. An interesting aspect of the liquid gallium can be seen near the end of the spread sequence after ~6 ms for all cases. At that time, the droplets see virtually no retraction of the contact line. They are pinned at maximum spread due to the adhesion of the oxide layer to the glass substrate. This is counterintuitive since static and dynamic advancing contact angles of the liquid metal both indicate it is nonwetting. This illustrates the complicated dynamic nature of the alloy mentioned previously.

VII. CONCLUSION

In summary we have conducted droplet impact experiments of a RTLM alloy consisting of 68.5% Ga, 21.5% In, and 10% Sn by weight over a range of Weber numbers, $10.7 \leqslant$ We $\leqslant 205.5$. In doing so we observed a strong correlation between the maximum spread parameter $\xi_{\max}$ and the impact velocity V_0, indicating a linear relationship which is an unusual relationship for droplet impacts. These impacts were modeled with a one-dimensional mass-spring approximation which affirmed the linear relationship between spread factor and impact velocity as well as independence of spread time and impact velocity. The stiffness associated with this model was chosen by directly measuring the stress response using a tensiometer and specially chosen cylindrical glass probe and was found to be 628 ± 37 mN/m, which we believe is the primary contributor to the force at the contact line. The effect of the oxidation is to change the wetting behavior. We performed a comparison of this model to existing models from Pasandideh-Fard *et al.* [22] and Clanet *et al.* [24] and noted that near lower Weber numbers around 10–80, $\xi_{\max}$ is lower for metal than the other models but begins to grow larger as the Weber number exceeds 100.

[1] D. Green Marques, P. Alhais Lopes, A. T. de Almeida, C. Majidi, and M. Tavakoli, Reliable interfaces for EGaIn multi-layer stretchable circuits and microelectronics, Lab Chip **19**, 897 (2019).

[2] J. Yan, Y. Lu, G. Chen, M. Yang, and Z. Gu, Advances in liquid metals for biomedical applications, Chem. Soc. Rev. **47**, 2518 (2018).

[3] T. Daeneke, K. Khoshmanesh, N. Mahmood, I. A. De Castro, D. Esrafilzadeh, S. J. Barrow, M. D. Dickey, and K. Kalantar-Zadeh, Liquid metals: Fundamentals and applications in chemistry, Chem. Soc. Rev **47**, 4073 (2018).

[4] M. D. Dickey, R. C. Chiechi, R. J. Larsen, E. A. Weiss, D. A. Weitz, and G. M. Whitesides, Eutectic gallium-indium (EGaIn): A liquid metal alloy for the formation of stable structures in microchannels at room temperature, Adv. Funct. Mater. **18**, 1097 (2008).

[5] E. Palleau, S. Reece, S. C. Desai, M. E. Smith, and M. D. Dickey, Self-healing stretchable wires for reconfigurable circuit wiring and 3D microfluidics, Adv. Mater. **25**, 1589 (2013).

[6] Y. Lin, J. Genzer, and M. D. Dickey, Attributes, fabrication, and applications of gallium-based liquid metal particles, Adv. Sci. **7**, 2000192 (2020).

[7] Geratherm Medical AG, Galinstan Safety Data Sheet, 2009.

[8] M. D. Dickey, Emerging applications of liquid metals featuring surface oxides, ACS Appl. Mater. Interfaces **6**, 18369 (2014).

[9] Q. Xu, N. Oudalov, Q. Guo, H. M. Jaeger, and E. Brown, Effect of oxidation on the mechanical properties of liquid gallium and eutectic gallium-indium, Phys. Fluids **24**, 063101 (2012).

[10] Q. Xu, E. Brown, and H. M. Jaeger, Impact dynamics of oxidized liquid metal drops, Phys. Rev. E **87**, 043012 (2013).

[11] C. Karcher, V. Kocourek, and D. Schulze, Experimental investigations of electromagnetic instabilities of free surfaces in a liquid metal drop, in *Proceedings of International Scientific Colloquium, Modelling for Electromagnetic Processing*, edited by E. Baake and B. Nacke (Leibniz University Hannover, Germany, 2003), pp. 105–110.

[12] T. Liu, P. Sen, and C. J. Kim, Characterization of nontoxic liquid-metal alloy Galinstan for applications in microdevices, J. Microelectromech. Syst. **21**, 443 (2012).

[13] J. W. Boley, E. L. White, and R. K. Kramer, Mechanically sintered gallium-indium nanoparticles, Adv. Mater. **27**, 2355 (2015).

[14] H. Li, S. Mei, L. Wang, Y. Gao, and J. Liu, Splashing phenomena of room temperature liquid metal droplet striking on the pool of the same liquid under ambient air environment, Int. J. Heat Fluid Flow **47**, 1 (2014).

[15] X. Jia, J. C. Yang, J. Zhang, and M. J. Ni, An experimental investigation on the collision outcomes of binary liquid metal droplets, Int. J. Multiphase Flow **116**, 80 (2019).

[16] C. Ladd, J.-H. So, J. Muth, and M. D. Dickey, 3D printing of free standing liquid metal microstructures, Adv. Mater. **25**, 5081 (2013).

[17] V. Kocourek, dissertation, Elektromagnetisches abstützen von flüssigmetall-tropfen, Master's thesis, Ilmenau University of Technology, Germany, 2008.

[18] G. H. Wagner and W. H. Gitzen, Gallium, J. Chem. Educ. **29**, 162 (1952).

[19] Geratherm Medical AG, Galinstan Safety Data Sheet, 2004, http://www.geratherm.com/wp-content/uploads/2010/02/Safety-Data-Sheet-Galinstan-2010-EN.pdf.

[20] B. Derby, Inkjet printing of functional and structural materials: Fluid property requirements, feature stability, and resolution, Annu. Rev. Mater. Res. **40**, 395 (2010).

[21] T.-M. Lee, T. G. Kang, J.-S. Yang, J. Jo, K.-Y. Kim, B.-O. Choi, and D.-S. Kim, Drop-on-demand solder droplet jetting system for fabricating microstructure, IEEE Trans. Electron. Packag. Manuf. **31**, 202 (2008).

[22] M. Pasandideh-Fard, Y. M. Qiao, S. Chandra, and J. Mostaghimi, Capillary effects during droplet impact on a solid surface, Phys. Fluids **8**, 650 (1998).

[23] V. Carey, *Liquid-Vapor Phase-Change Phenomena*, 2nd ed. (Taylor and Francis, New York, 2008).

[24] C. Clanet, C. Beguin, D. Richard, and D. Quere, Maximal deformation of an impacting drop, J. Fluid Mech. **517**, 199 (2004).

[25] D. Richard, C. Clanet, and D. Quéré, Contact time of a bouncing drop, Nature (London) **417**, 811 (2002).

[26] Y. Lin, C. Ladd, S. Wang, A. Martin, J. Genzer, S. A. Khan, and M. D. Dickey, Drawing liquid metal wires at room temperature, Extreme Mech. Lett. **7**, 55 (2016).

[27] S. Schiaffino and A. A. Sonin, Molten droplet deposition and solidification at low Weber numbers, Phys. Fluids **9**, 3172 (1997).

[28] G. Kelly, *Fundamentals of Mechanical Vibrations*, 2nd ed. (McGraw-Hill, New York, 2000).

[29] S. Chandra, Droplet impact on solid surfaces, in *Droplet and Spray Transport: Paradigms and Applications*, edited by S. Basu, A. K. Agarwal, A. Mukhopadhyay, and C. Patel (Springer, Singapore, 2018), pp. 299–310.